

ISSN: 0149-6395 (Print) 1520-5754 (Online) Journal homepage: <https://www.tandfonline.com/loi/lst20>


Effects of calcination temperature on organic functional groups of TiO_2 and the adsorption performance of the TiO_2 for methylene blue

Jiangtao Feng, Yunpeng Liu, Lin Zhang, Jinwei Zhu, Jie Chen, Hao Xu, Honghui Yang & Wei Yan

To cite this article: Jiangtao Feng, Yunpeng Liu, Lin Zhang, Jinwei Zhu, Jie Chen, Hao Xu, Honghui Yang & Wei Yan (2020) Effects of calcination temperature on organic functional groups of TiO_2 and the adsorption performance of the TiO_2 for methylene blue, Separation Science and Technology, 55:4, 672-683, DOI: [10.1080/01496395.2019.1574822](https://doi.org/10.1080/01496395.2019.1574822)


To link to this article: <https://doi.org/10.1080/01496395.2019.1574822>

 View supplementary material 

 Published online: 12 Feb 2019.

 Submit your article to this journal 

 Article views: 38

 View related articles 

 View Crossmark data 



Effects of calcination temperature on organic functional groups of TiO₂ and the adsorption performance of the TiO₂ for methylene blue

Jiangtao Feng^a, Yunpeng Liu^a, Lin Zhang^a, Jinwei Zhu^{a,b}, Jie Chen^a, Hao Xu^a, Honghui Yang^a, and Wei Yan^a

^aDepartment of Environmental Science and Engineering, Xi'an Jiaotong University, Xi'an, P.R. China; ^bShaanxi Electrical Equipment Institution, Xi'an, P.R. China

ABSTRACT

Herein, TiO₂ was prepared by the hydrolysis method in citric acid (with both carboxyl and hydroxyl groups) solution firstly. And then, the as-prepared TiO₂ was calcined at 50, 150, 250, 350, and 450°C, respectively, in order to investigate the effects of the calcination temperature on the physicochemical property and the adsorption performance of TiO₂. The adsorption performance of the prepared TiO₂ samples for cationic dye-Methylene Blue (MB) was also studied. The results indicated that high calcination temperature can destroy the organic moieties on the TiO₂ samples and further influence the adsorption performance of TiO₂ for the removal of cationic dye-MB.

ARTICLE HISTORY

Received 29 January 2018
Accepted 22 January 2019

KEYWORDS

Titanium dioxide (TiO₂);
calcination; functional
groups; methylene blue
(MB); adsorption

Introduction

In recent years, there has been growing interest in the field of organic contaminant removal by adsorption.^[1–4] The adsorption process is often used to remove organic dyes due to its low cost, simplicity in operation, the abundant raw material source, nontoxicity, and acceptable removal efficiency.^[5,6] The adsorption behavior of the adsorbent varies dramatically with different performances in dye wastewater. Meanwhile, the adsorption capacities of the adsorbent for dyes are mainly affected by the surface physicochemical properties of the adsorbent.^[2,7] For instance, the functional groups on the surface of activated carbon (AC) play a key role in the adsorption performance.^[8] And the activated carbon modified by H₂O₂ oxidation to formed carbonyl, lactonic, and carboxylic groups on the surface, has a higher adsorption affinity to ibuprofen than that of the pristine AC.^[9] The commercial AC with the alkaline surface, modified by thermal treatment under H₂ flow at 700°C, was in favor of the adsorption for anionic dye (reactive red 241).^[10]

Titania (TiO₂), as an inexpensive and non-toxic material, has been used as photocatalyst in the energy and environmental field. However, the adsorption of pollutants from the bulk solution to the surface of TiO₂ is a key role for the effective photodegradation when TiO₂ is used as a photocatalyst.^[11,12] Nowadays, more

and more attention has been focused on the adsorption of TiO₂ for different pollutants. Furthermore, many researchers studied the surface modification of TiO₂ by altering its surface physicochemical properties to improve the adsorption performance. It was reported by Janus et al.^[13] that the carbon modification can enhance the adsorption capacity of TiO₂ for Direct Green 99 to 96.77 mg/g, which was more than that of the unmodified TiO₂. It was found the surface-fluorinated TiO₂ (F-TiO₂) particles had different adsorption modes of Rhodamine B (RhB) dye from those of pure TiO₂. The adsorption group of the pure TiO₂ for RhB was the carboxylic (-COOH) group, while RhB was switched to preferentially anchor on F-TiO₂ through the cationic moiety (-NEt₂ group).^[14] The mesoporous TiO₂ with carboxylate groups functionalized by ethylenediaminetetraacetic acid (EDTA) exhibited an enhanced adsorption capacity for removing MB (32.15 mg/g) from aqueous solution.^[15] The aim of all the modification methods are to increase the adsorption capacity of TiO₂ by creating more functional groups (-COOH, -OH, -NH₂, etc.) onto it. In consideration of the abundant functional groups (-COOH and -OH) in citric acid molecule (Fig. 1), many researches used the compounds contained citric acid and TiO₂ particle to adsorb pollutant from wastewater.^[16–18] Meanwhile, calcination temperature could change the



Figure 1. Molecules of CA and MB.

quantity of organic functional groups of TiO_2 ,^[19] and then had an influence on the adsorption performance in theory. However, in most reports, researchers prepared surface functionalized TiO_2 at only low temperature (under 100°C)^[20,21] to study the adsorption performance of the modified TiO_2 . The surface physicochemical properties and the adsorption performance of TiO_2 impacted by the different calcination temperatures are rarely investigated. Thus, citric acid based studies, could be considered to be the good analogues for the effect of functional groups on adsorption capacity, which can provide insight into the adsorption mechanisms of the quantity of functional groups.

Herein, TiO_2 samples prepared in carboxylic acid solution by sol-gel method were calcined at the different temperatures to study the effects of calcination temperature on the surface physicochemical properties and the adsorption performance of TiO_2 . It was found that the organic moieties on the surface of TiO_2 decreased with the calcination temperature increasing. Furthermore, the adsorption capacity of TiO_2 for MB was also reduced with the increase of calcination temperature.

Experimental details

Materials

Tetrabutyl titanate (TBOT, 340.36 g/mol, 98%), Citric Acid (CA, 192.14 g/mol, 99%), n-propanol were of analytical grade (Sinopharm Chemical Reagent Co., Ltd., Shanghai, China). Cationic dye Methylene Blue (MB, 319.86 g/mol) was purchased from Beijing Chemical Reagent Co., China. The structures of CA and MB are shown in Fig. 1. The deionized water used in this study was obtained from the EPED-40TF Superpure Water System (EPED, China).

Preparation of TiO_2 samples

TiO_2 samples were synthesized by the hydrolysis method. A typical pathway was as follows: firstly, a mixture of TBOT and n-propanol (the volume ratio

is 5:2) was slowly added into 200 mL Citric Acid solution (0.16 mol/L) with magnetic stirring for 2 h at 65°C . Then the suspension was stirred for another 12 h under the ambient temperature. Finally, the white solid had been filtrated and rinsed several times with water until the pH value of the washing solution became neutral. The filter residue was dried with air-seasoning for 24 h. And then, the as-prepared TiO_2 powder was calcined at different temperatures of 50°C , 150°C , 250°C , 350°C , and 450°C for 2 h, respectively. The as-prepared TiO_2 samples were named as T-50, T-150, T-250, T-350, and T-450 according to the calcination temperature.

Characterizations of TiO_2 samples

Fourier Transform Infrared spectra (FT-IR) of the samples were conducted on BRUKER TENSOR 37 FT-IR spectrophotometer in the range of $4000\text{--}400\text{ cm}^{-1}$ by the KBr pellet method. BET surface area (S_{BET}), total pore volume (V), and average pore radius (R) were measured at 77 K using Builder SSA-4200 (Beijing, China). Zeta potentials were tested with Malvern Zetasizer Nano ZS90. Samples for zeta potential measurement were prepared by adding 5 mg of TiO_2 into 10 mL NaCl solution (10^{-3} mol/L) at different pH values from 2 to 12 (adjusted with 0.1 mol/L HNO_3 or NaOH solution). X-ray diffraction patterns of samples were obtained with an X'Pert PRO MRD Diffractometer using Cu-K α radiation. The morphology and elemental information were obtained on a scanning electron microscopy (SEM, JSM-6700F, Japan) with an energy dispersive X-ray spectroscopy (EDX).

Boehm titration

The organic acidic and basic groups on the as-prepared TiO_2 samples were studied by the Boehm titration method. In the titration process, the TiO_2 samples were firstly equilibrated in HCl solution (0.01 mol/L) for 3 d, and then washed with deionized water until it was free of Cl^- detected by AgNO_3 solution. The dried

TiO₂ samples (0.5 g) was dispersed in 25 mL of the 0.05 mol/L solution of NaHCO₃, NaOH, or HCl solution to form suspensions and shaken for 24 h. The excess of base or acid in 10 mL of the filtrate was titrated with 0.01 mol/L HCl or NaOH solution, respectively. Surface acidity and basicity were calculated by the assumption that NaHCO₃ neutralizes carboxyl groups only, NaOH neutralizes all acidic groups and HCl neutralizes all basic groups.

Adsorption experiments

The adsorption of MB was carried out by shaking the mixture of solution with as-prepared TiO₂ samples (2.0 g/L) at 25°C. Then the suspension was centrifuged at 4000 rpm for 6 min. The supernatant was analyzed by the UV-Vis spectrophotometer (Agilent 8453) and the absorbance value was read at the wavelength of 665 nm, in order to evaluate the adsorption capacity of MB onto TiO₂.

The amount of MB molecules adsorbed onto the as-prepared TiO₂ samples Q_t (mg/g) at a certain time t was calculated from Eq. (1):

$$Q_t = \frac{C_0 - C_t}{M} \times V \quad (1)$$

where C_0 (mg/L) is the initial concentration of the MB solution; C_t (mg/L) is the residual concentration of the MB solution at time t (min); V (L) is the solution volume; and M (g) is TiO₂ sample mass.

The adsorption equilibrium of MB (100, 300, and 500 mg/L) was conducted at 25°C. Adsorption isotherms of MB were obtained by mixing different concentrations (10–900 mg/L) of MB solution with 2 g/L of as-prepared TiO₂ samples, and then the solution was shaken for 120 min in dark at 25°C. The Langmuir, Freundlich and Dubinin-Radushkevich (D-R) isotherm models were described according to Eqs. (2)–(4), respectively: [22–25]

$$Q_t = \frac{Q_{\max} K_L C_t}{1 + K_L C_t} \quad (2)$$

$$Q_t = K_F C_t^{1/n} \quad (3)$$

$$\ln Q_t = \ln Q_{\max} - \frac{1}{2E^2} [RT \ln(1 + 1/C_t)]^2 \quad (4)$$

where Q_{\max} (mg/g) is the maximum monolayer molecular adsorption capacity onto the adsorbent in Langmuir isotherm model; K_L (L/mg) and K_F (mg^{1–n}·Lⁿ/g) are the constant of Langmuir and Freundlich isotherm model, respectively. $1/n$ represents the degree of adsorption

dependence on equilibrium concentration in Freundlich isotherm model; E (kJ/mol), R (8.314 J/(mol·K)) and T (K) of D-R isotherm model formula are the mean Gibbs free adsorption energy, the gas constant and the temperature of this adsorption system, respectively.

In addition, the dimensionless separation factor R_L , an essential characteristic of the Langmuir model to reflect the favorability of an adsorption process, is expressed as: [26–28]

$$R_L = \frac{1}{1 + K_L C_m} \quad (5)$$

where C_m (mg/L) is the maximum initial concentration of MB in solution.

The adsorption kinetics experiments were conducted at 25°C in dark. Adsorption kinetics of MB were obtained by mixing 1000 mg/L MB solution with 2 g/L of as-prepared TiO₂ samples, and then the solution was shaken for 120 min at 25°C, and sampled at regular intervals. The pseudo-first-order, pseudo-second-order and Elovich models were described according to Eqs. (6)–(8), respectively: [29–31]

$$Q_t = Q_e (1 - e^{-k_1 t}) \quad (6)$$

$$Q_t = \frac{k_2 Q_e^2 t}{1 + k_2 Q_e t} \quad (7)$$

$$Q_t = \frac{1}{\beta} \ln(\alpha\beta) + \frac{1}{\beta} \ln(t) \quad (8)$$

where k_1 (min^{–1}) and k_2 (g/(mg·min)) are successively the rate constants for the pseudo-first-order and pseudo-second-order; α (mg/(g·min)) and β (g/mg) of the Elovich model formula are initial sorption rate and desorption constant, respectively. Q_t (mg/g) is the amount adsorbed at time t (min), and Q_e (mg/g) is the equilibrium adsorption capacity.

The influence of the pH on the adsorption capacities was investigated by adjusting the pH of 1000 mg·L^{–1} MB solution with NaOH or HCl solution (pH = 2.0–12.0). Then the 40 mg TiO₂ samples were employed to treat MB solutions with different pH. The thermodynamics of the prepared adsorbent was examined by changing the adsorption temperature from 25 to 45°C

Results and discussion

Characterizations of TiO₂ samples

The FT-IR spectra of TiO₂ samples calcined under various temperatures are shown in Fig. 2. The copious

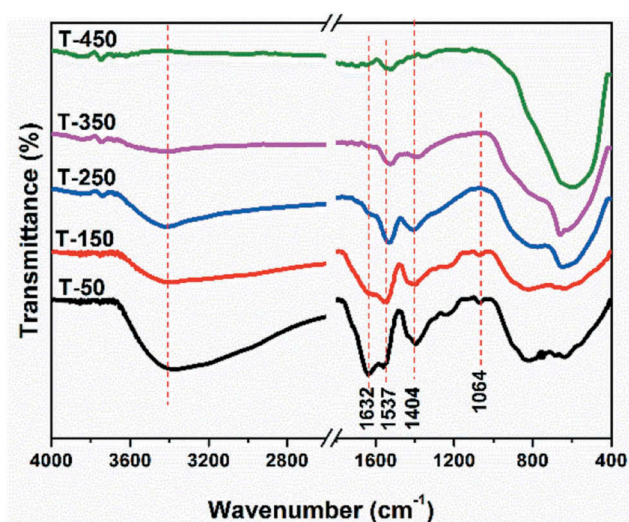


Figure 2. FT-IR spectra of TiO₂ samples.

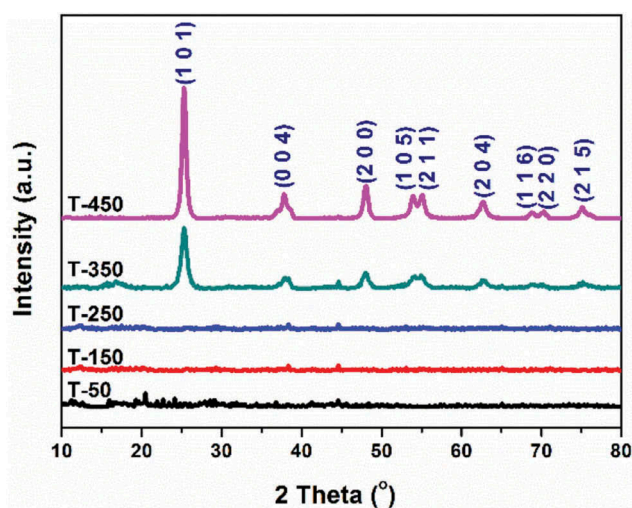


Figure 3. X-ray diffraction patterns of TiO₂ samples.

surface groups in the TiO₂ samples calcined under lower temperatures (50, 150, 250°C) appear in the spectra. In these spectra, the broad peak in the range of 3000–3500 cm⁻¹ is attributed to the vibration of -OH. And the bond at 1632 cm⁻¹ is characteristic to the bending vibration of the adsorbed water; the bands at 1537 and 1392 cm⁻¹ are related to the asymmetric and symmetric stretching vibrations of carboxyl, respectively. The value of $\Delta\nu$ (COO⁻) for the TiO₂ samples at lower calcined temperature was approximate 145 cm⁻¹, illustrating a bridging structure between TiO₂ and Citric Acid.^[32,33] The bond at 1225 cm⁻¹ is due to the stretching vibration of C-O, and the bond at 1070 cm⁻¹ assigns to the bending of C-H.^[32] Out-of-plane bending of C-C and C-H are in the range of 600–900 cm⁻¹.^[34,35] These bonds appeared in the

spectra of the TiO₂ samples calcined under lower temperatures (below 250°C), indicating that the as-prepared TiO₂ samples have copious functional groups on their surface, which would be favor to the adsorption of the samples. The characteristic peaks delegated organic phase became weak and further disappeared with the increase of the calcination temperature. For instance, the bond of -OH in the spectra of T-250 sample is quite weak. Above 250°C, the bands belong to -OH, C = O, C-C, and C-H completely disappeared. Only the vibration bonds (1562 and 1392 cm⁻¹) of carboxyl^[36–40] exist there and then become weaker and weaker with the increase of the calcination temperature, indicating the better stability of carboxyl than that of other groups in the TiO₂ samples at higher temperature. These phenomena are due to decomposition of the organic groups (from citric acid, propanol and the butanol from the hydrolysis process of TBOT) in the TiO₂ samples at higher temperature. However, the broad bond delegated the vibration of O-Ti-O at 400–700 cm⁻¹^[41–43] becomes obvious after the calcination temperature increases above 350°C. Thus, different functional groups are in the TiO₂ samples under various calcination temperatures, which will further influence the adsorption performance of the samples.

The organic groups, especially the oxygen-containing functional organic groups on the surface of samples, give rise to an apparent surface acidity/basicity of the material. Furthermore, the surface acidity/basicity would violently affect the adsorption performance of the material.^[44] Therefore, the Boehm titration was used to test the surface acidity/basicity of the as-prepared TiO₂ samples and the results are presented in Table 1. The data illustrate that the carboxyl acidity decreased with the increasing calcination temperature, and the total acidity declined in the same trend. However, the basicity takes on an opposite trend, which increased with the increasing temperature. All the high-temperature (> 250°C) samples reveal lower acidity and total acidity/basicity value but higher basicity than that of the low-temperature (≤ 250°C) samples. The decline of carboxyl groups and acidity with the increasing temperature illustrate that the low-temperature samples are more organic in nature.

Table 1. Boehm titration results and the surface density for functional groups of TiO₂ samples.

Sample	Boehm titration (mmol/g)			
	Carboxyl	Acidic	Basic	All
T-50	2.96	3.65	0.04	4.36
T-150	2.67	3.06	0.05	3.51
T-250	1.93	2.37	0.07	3.13
T-350	0.60	1.51	0.11	1.62
T-450	0.45	1.13	0.40	1.53

More surface functional organic groups indicate more polar nature of the samples in keeping with their adsorption capacity.^[45]

The BET surface area (S_{BET}), pore volume (V_p) and pore diameter parameters are shown in Table 2. The S_{BET} and pore diameter were calculated from the corresponding nitrogen adsorption-desorption isotherms and the desorption branch of the nitrogen isotherms by the BJH ((Barrett-Joyner-Halenda) method, respectively (Fig. S1). It can be seen from the data that the S_{BET} of the amorphous TiO_2 is smaller than that of the crystalline TiO_2 samples. It can be explained by the fact that the S_{BET} of the TiO_2 samples greatly depends on the size of the aggregated TiO_2 nanoparticles. The V_p also experienced the similar variation tendency except that of the bulk sample calcined at 350°C , which is mainly due to the agglomeration of materials for the melting of organic components at high temperature. This is ascribed to the collapse of the porous structure, and the phase transformation.^[46] The sharp decline in desorption curve for the low temperature samples is indicative of mesoporosity. Furthermore, the hysteresis between the adsorption and desorption curves for the high-temperature samples illustrated the diffusion bottleneck in the tissue of the samples, probably owing to heterogeneous pore size. The pore radius of the samples calculated by the BJH method was in a narrow range of 3.0–15 nm, which indicates that all the as-prepared samples have mesoporous structures. Such structures are the results of the pores which are formed between TiO_2 particles.^[47]

It is reported that the organic matter could be destroyed by the increasing calcination temperature.^[48] In this study, the content of each element was calculated by EDX (Table 3 and Fig. S2). The degree of the organic group may be described by the molar C/Ti, because C is primarily associated with organic matter in the samples. The higher C/Ti ratio for T-50 (C/Ti = 1.77), T-150 (C/Ti = 1.32) suggests that these samples contain a great amount of organic residues, which is apparently caused by the low calcination temperature. On the one hand, the organic moieties in these two samples preserve certain original organic structures,

Table 2. Textural properties of the TiO_2 samples.

Sample	S_{BET} (m^2/g)	V_p (cm^3/g)	r (nm)
T-50	4.264	0.015	6.6
T-150	3.321	0.029	15.0
T-250	7.748	0.028	8.6
T-350	12.840	0.022	3.9
T-450	17.570	0.033	3.3

Table 3. The molar ratio of different atoms on the TiO_2 samples.

Sample	C/%	O/%	Ti/%	Molar (O/Ti)	Molar (C/Ti)
T-50	25.30	60.37	14.33	4.21	1.77
T-150	22.33	60.69	16.98	3.57	1.32
T-250	16.53	62.24	21.23	2.93	0.78
T-350	8.67	59.00	32.33	1.82	0.27
T-450	4.19	63.69	32.12	1.98	0.13

such as carboxyl and hydroxyl, according to the FT-IR spectra. On the other hand, the C/Ti ratio decreases dramatically with the increase of temperature, especially when the temperature is over 250°C . The C/Ti ratio is stable around 0.10 after the calcination temperature is over 350°C . Such a low value illustrates that there are hardly organic groups in the sample, which is consistent with the results of FT-IR and Boehm titration.

The XRD pattern (Fig. 3) shows that the crystalline phase of each sample varies with the calcination temperature increasing. As well as we known, the high calcination temperature is beneficial to the crystallization of TiO_2 .^[49] So we can see from the XRD patterns that the crystallographic phase of the samples calcined under 250°C is amorphous, the samples calcined at 350°C and 450°C belong to the anatase type, which shows the preferential orientation for anatase in the (101) direction (corresponding $2\theta = 25.33^\circ$). This fact suggests that the phase transformation from amorphous to anatase for the as-prepared TiO_2 samples occurs at *ca.* 300°C . This phenomena indicates that almost all organic moiety preventing crystallization were completely removed from the samples at 350°C , which is consistent with the results of EDX.

The morphologies of the as-prepared TiO_2 samples are observed by SEM (Fig. S2). The sample without calcination is composed by the microparticle. With the calcination temperature increasing, the diameter of the particle increased until the temperature is 350°C . The morphology of the TiO_2 sample calcined at 350°C is blocky. This results from the fusion of the samples with organic moieties in the calcination procedure. When the calcination temperature is over 350°C – 450°C , the morphology of the sample becomes micro particles again. The organic moiety prevents the amorphous TiO_2 particles from aggregating into larger ones and further affects the formation of TiO_2 crystal.^[50] After the organic moiety was removed by calcination, the morphology of the samples takes on microparticle again. In a word, the variation of the functional groups, crystal phase, morphology, BET surface area and pore diameter would affect the physico-chemical properties of the TiO_2 samples, especially the adsorption performance.

Adsorption results of TiO₂ samples for MB

Effect of time

The as-prepared TiO₂ samples were applied for MB adsorption. The relative curves for the adsorption time to the adsorption capacity of MB at different initial concentrations illustrated the adsorption equilibrium time is correlation with the increasing calcination temperature (Fig. S3). For instance, the adsorption equilibrium can be achieved within 30 min for T-50 and T-150. Moreover, the equilibrium was extended to 60 min for both T-350 and T-450. This might be for the loss of organic groups on TiO₂ samples at higher temperature. Therefore, the contact time of the adsorption isotherm was maintained 120 min in the follow experiments.

Effect of pH

The effect of pH on adsorption capacities of T-50 to T-450 are shown in Fig. S4. It can be observed that the adsorption capacities of the five adsorbents were positively affected by the solution pH, and increased with pH. Meanwhile, all of samples have better adsorption performance in alkaline condition. In order to analyze this phenomenon, the zeta potential change trend varying with the pH increase of the as-prepared TiO₂ samples is shown in Fig. 4. The isoelectric point (pH_{pzc}) is the pH value when the zeta potential value is zero. The pH_{pzc} values of the TiO₂ samples are from approximately 2.0 to 7 with the calcination temperature increasing ($\text{pH}_{\text{pzc(T-50)}} = 6.93$, $\text{pH}_{\text{pzc(T-150)}} = 6.19$, $\text{pH}_{\text{pzc(T-250)}} = 4.70$, $\text{pH}_{\text{pzc(T-350)}} = 3.95$, and $\text{pH}_{\text{pzc(T-50)}} = 2.34$). The zeta potential of the TiO₂ samples at lower calcination temperature exhibited negative zeta potential at lower pH value. This can be

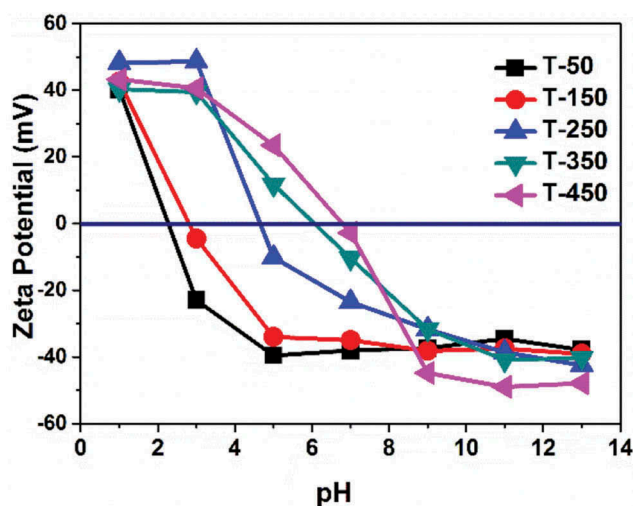


Figure 4. Zeta potential of TiO₂ samples.

deduced that the organic moieties, especially carboxyl groups from citric acid on the TiO₂ samples make the surface negatively charged. The TiO₂ samples are gradually positively charged while the calcination temperature increased, which results from the loss of the carboxyl groups at higher temperature. However, the zeta potential change would affect the interaction between the TiO₂ samples and the adsorbates.^[51]

Evaluation of adsorption isotherm models

The effects of MB concentration on the adsorption capacity of the five adsorbents were investigated and the results are illustrated in Fig. 5(a), showing that all the Q_e of the five adsorbents goes up steadily as the initial concentration of MB solution increase. This is probably because when the concentration of MB increases, the driving force of diffusion increases due to the higher concentration gradient. However, as the adsorption sites on the adsorbents reduce with increasing adsorption value, the further increase of Q_e with is slowed down. Meanwhile, the Langmuir, Freundlich and D-R adsorption isotherm models were employed to describe the interaction between the adsorbate and the adsorbent, the adsorption isotherm at 25°C was investigated. The corresponding experimental data, Langmuir fit, Freundlich fit and D-R fit were shown in Fig. 5. The fitting parameters of the Langmuir, Freundlich and D-R models are listed in Table 4. Comparing to the fitted parameters of the models, especially the correlation coefficient (R^2), Langmuir model is more favorable to describe the adsorption process of MB onto the as-prepared TiO₂ samples, which indicates that the adsorption sites on the TiO₂ samples are finite and the adsorption of MB onto the surface of the TiO₂ samples is a monolayer adsorption process. Moreover, the values of R_L are in the range of 0–1.0, and the values of $1/n$ are centered in the range of 0.3–0.6, suggesting that the adsorption is favorable.

According the Langmuir fitting results, as shown in Fig. 5(b), the adsorption capacity decreased in the order of the T-50 to T-450, which indicates that the MB adsorption by the TiO₂ samples decreased with the calcination temperature increasing. The adsorption capacity of the amorphous TiO₂ samples (calcined at lower temperatures) exhibited the higher affinity to MB than that of the crystalline TiO₂ (calcined at higher temperatures), which is similar to Nguyen-Le and Kim's reports.^[15,51] Meanwhile, the adsorption capacity of MB onto T-50 was higher than in a study previously reported on that of other adsorbents (listed in Table 5), indicating the as-prepared T-50 was a promising excellent adsorbent.^[52–58]

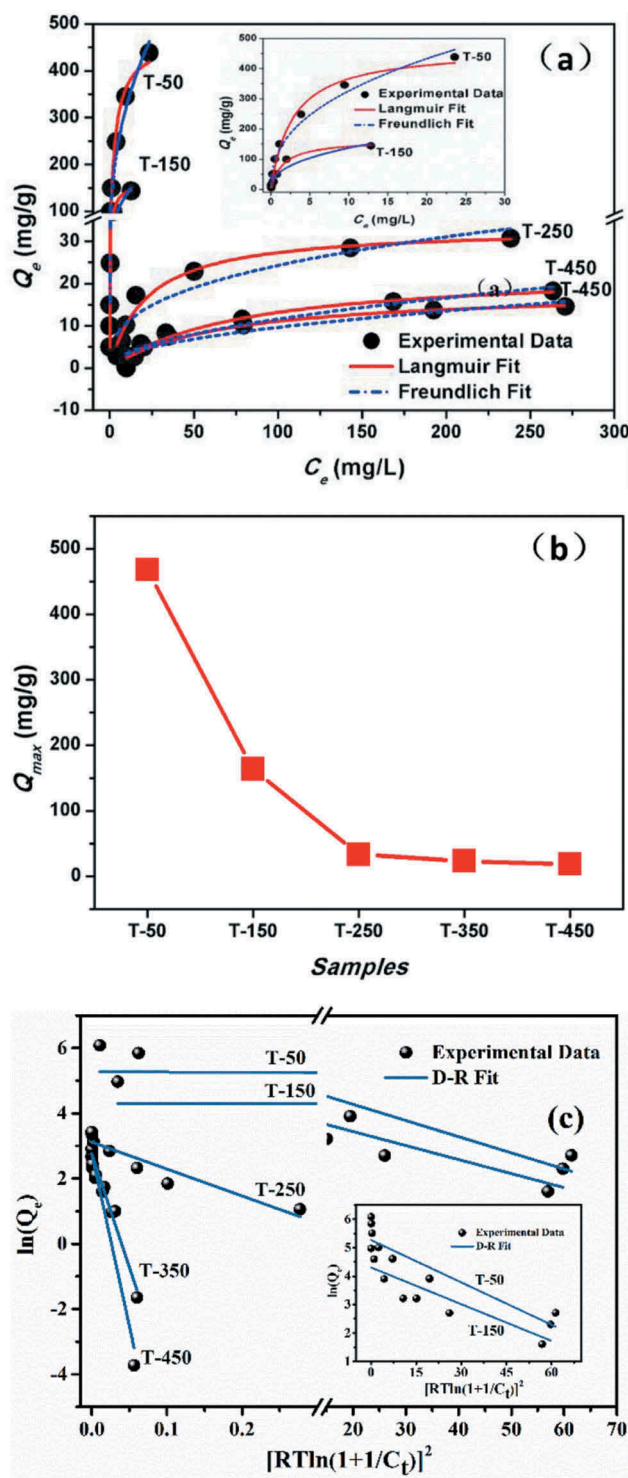


Figure 5. Langmuir and Freundlich fitted adsorption isotherms of samples (a): inset is the isotherms for T-50 and T-150; and the maximum adsorption capacities of samples from Langmuir Fit (b). D-R fitted adsorption isotherms of samples (c): inset is the isotherms for T-50 and T-150.

Adsorption kinetics

Fig. 6 shows the adsorption kinetics of MB on TiO₂ samples. It is obvious that the adsorption equilibrium of MB on T-50 samples could be achieved in 15 min, indicating the

as-prepared T-50 was a promising excellent adsorbent. The relevant parameters of the adsorption kinetics models were calculated and are listed in Table 6. It can be observed that the correlation coefficients of the pseudo-first-order model ($R^2 = 0.9921\text{--}0.9989$) was more appropriate to describe the adsorption kinetics of the five kinds of TiO₂ samples for MB than the pseudo-second-order model ($R^2 = 0.9815\text{--}0.9928$) and the Elovich model ($R^2 = 0.8578\text{--}0.9667$). Meanwhile, the calculated values of Q_{eq} which derived from the pseudo-first-order model matched well with the experimental data. Therefore, the adsorption kinetics of MB on the five kinds of TiO₂ samples followed the pseudo-first-order model, which indicates that the adsorption process of MB onto TiO₂ samples appears to be controlled by the diffusion process. [59]

Effect of temperature

The values of thermodynamic parameters, including the Gibb's free energy change (ΔG), enthalpy change (ΔH), and entropy change (ΔS), can be calculated from the following Eqs. (9) and (10):

$$\Delta G = -RT \ln K_L \quad (9)$$

$$\ln K = \frac{\Delta S}{R} - \frac{\Delta H}{RT} \quad (10)$$

where ΔG (kJ/mol) is the Gibb's free energy change of adsorption, K_L is the Langmuir constant, R (8.314 J/(mol·K)) is the universal gas constant, T is the temperature in K, ΔS is entropy change (J/(mol·K)), and ΔH is the enthalpy change (kJ/mol). The ΔH and ΔS values can be calculated from the slope and intercept of a linear plot of $\ln K$ versus $1/T$. The obtained values of ΔG , ΔH , and ΔS which indicate the adsorption of MB onto the five adsorbents under different temperatures are listed in Table 7.

The positive values of ΔH confirm the endothermic nature of adsorption process of MB onto the five adsorbents. The positive values of ΔS reveal that the possibility of increasing randomness at the solid liquid interface occurs in the adsorption of MB onto the five adsorbents. For T-50, the negative values of ΔG indicate that the process is feasible and spontaneous, but for other samples, the values of ΔG are negative which reveal that the process is feasible but nonspontaneous. [60] Meanwhile, with regards to the adsorption of MB onto every sample, the values of ΔG of the five adsorbents are becoming more and more negative with the increase of temperature, which suggest that the higher temperature may facilitate the adsorption of MB onto the five adsorbents. [61,62]

Table 4. Parameters of Langmuir, Freundlich and D-R adsorption isotherm models.

Samples	Langmuir model parameters				Freundlich model parameters			D-R model parameters		
	Q_{\max} (mg/g)	K_L (L/mg)	R_L	R^2	K_F ($\text{mg}^{1-n} \cdot \text{L}^n \cdot \text{g}^{-1}$)	$1/n$	R^2	Q_{\max} (mg/g)	E (kJ/mol)	R^2
T-50	468.24	0.358	0.0031–0.0852	0.9972	127.369	0.408	0.8661	194.03	4.489	0.6440
T-150	163.36	0.640	0.0052–0.1351	0.9904	53.706	0.406	0.9143	73.85	4.822	0.7859
T-250	33.39	0.045	0.1000–0.6897	0.9634	4.747	0.355	0.8682	22.55	0.348	0.8721
T-350	23.30	0.013	0.2041–0.8850	0.9578	1.055	0.521	0.9142	15.68	0.120	0.9684
T-450	18.46	0.015	0.1718–0.8696	0.9479	1.019	0.488	0.8812	16.02	0.097	0.9359

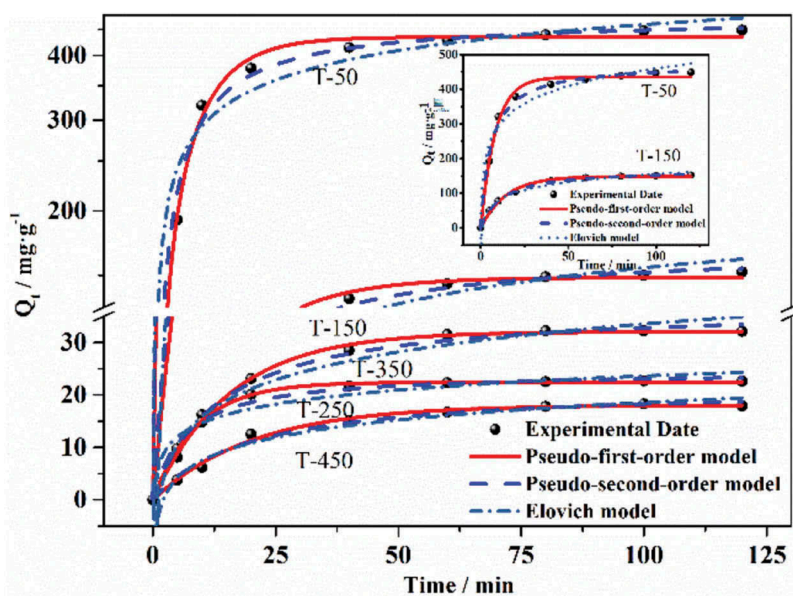
Table 5. Adsorption comparison of T-50 and reported studies on adsorbents for MB.

Adsorbent	Q_{\max} (mg/g)	Reference
T-50	468.24	This work
Ruthenium nanoparticle-loaded activated carbon	41.64	[52]
Purified palygorskite	55.0	[53]
Tartaric acid modified wheat bran	25.18	[54]
Fe ₂ O ₃ nanocrystals-anchored macro/mesoporous graphene	216.3	[55]
Al ₂ O ₃ nanoparticle	229.1	[56]
Unburned carbon	79.8	[57]
Fly ash	3.6	[58]

Regeneration

From practical point of view, repeated availability was an important factor for an advanced adsorbent. The

regeneration and reuse of the five adsorbents for MB removal were also evaluated. The regeneration of the five adsorbents were achieved by using HCl solution (0.1 mol·L⁻¹) as desorption agent and NaOH solution (0.1 mol·L⁻¹) as the activation agent. Repeatedly, the regenerated adsorbents were utilized to treat MB solution to study the regeneration stability of the five adsorbents. The results are summarized in Fig. S5. After five cycles, the T-50 and T-150 were still as active as the original samples maintaining intrinsic adsorption capacities of MB. However, it is obvious that the adsorption capacity of MB onto T-250, T-350, and T-450 have a sharp drop and the decrease degree of adsorption capacity aggravate with the debasement of calcine temperature. These phenomena indicate that

**Figure 6.** Adsorption kinetics plots of MB onto TiO₂ samples: inset is the kinetics for T-50 and T-150.**Table 6.** Parameters of kinetic models for MB adsorption on TiO₂ samples.

Sample	Pseudo-first-order model			Pseudo-second-order model			Elovich model		
	k_1 (min ⁻¹)	q_e (mg/g)	R^2	k_2 (g/(mg·min))	q_e (mg/g)	R^2	a (mg/(g·min))	β (g/mg)	R^2
T-50	0.120	435.06	0.9922	0.3571	474.75	0.9920	400.778	0.0137	0.8777
T-150	0.069	148.65	0.9936	0.0499	170.02	0.9928	35.568	0.0301	0.9667
T-250	0.064	32.06	0.9971	0.0202	37.15	0.9913	6.059	0.1304	0.9445
T-350	0.111	22.43	0.9989	0.0639	24.52	0.9903	17.345	0.2586	0.8578
T-450	0.049	18.05	0.9921	0.0240	21.76	0.9851	2.297	0.2084	0.9560

Table 7. Thermodynamic parameters for the adsorption of MB onto TiO₂ samples.

Sample	$\Delta H/\text{kJ}\cdot\text{mol}^{-1}$	$\Delta S/\text{J}\cdot\text{K}^{-1}\cdot\text{mol}^{-1}$	$\Delta G/\text{kJ}\cdot\text{mol}^{-1}$
T-50	18.61	66.21	25°C -1.121
			35°C -1.783
			45°C -2.445
T-150	9.37	25.95	25°C 1.637
			35°C 1.377
			45°C 1.118
T-250	14.02	25.33	25°C 6.472
			35°C 6.218
			45°C 5.965
T-350	11.94	13.31	25°C 7.974
			35°C 7.841
			45°C 7.707
T-450	7.94	3.76	25°C 6.820
			35°C 6.782
			45°C 6.744

T-50 and T-150 which have more functional groups than TiO₂ in other calcine temperature (T-250, T-350, and T-450) could be the excellent candidate for the treatment of MB pollution. The other samples (T-250, T-350, and T-450) have relatively low regeneration stability due to the lack of functional groups, and it is difficult to desorbed and excited by acid-base solutions.

The characterizations of TiO₂ samples after adsorption of MB

The SEM of TiO₂ of T-50 to T-450 after adsorption of MB was presented in Fig. S6, and there no remarkable changes of morphology before and after adsorption. The morphology of T-350 still maintain blocky structure after adsorption of MB, but the subtle changes of the other adsorbents could be observed in Fig. S6 (a, b, c, and e). Compared with the morphology before adsorption, the particle of T-50, T-150, T-250, and T-450 began to lump after adsorption. Sectional particle formed block when the particles were held together by weak surface forces (soft agglomeration) such as van der Waals or capillary forces or by strong chemical bonds (hard agglomeration).^[63] The XRD spectra of T-50 to T-450 after adsorption of MB are shown in Fig. S7. It can be seen that the T-350 and T-450 still belong to anatase-type which shows no peak shift, and the crystallographic phase of the samples calcined at other temperature remain amorphous after adsorption. Hence, the adsorption process of MB has no effect on the crystallographic phase of TiO₂.

Table 8. The molar ratio of different atoms on the TiO₂ samples after adsorption of MB.

Sample	C/%	O/%	Ti/%	Molar (O/Ti)	Molar (C/Ti)
T-50	37.38	52.68	9.89	5.34	3.78
T-150	26.44	60.74	12.8	4.74	2.07
T-250	26.29	51.11	22.41	2.28	1.17
T-350	14.12	43.73	42.15	1.04	0.36
T-450	8.82	63.96	27.23	2.35	0.32

In order to observe the change of element content before and after adsorption, the EDX was also carried out again (Table 8 and Fig. S6). In Fig. S6, the presence of N, Cl and S elements indicate that the MB are adsorbed onto the surface of T-50 to T-450. And in Table 8, the C/Ti ratio of the five adsorbents are higher than that of original samples, meanwhile, the change extent of C/Ti ratio gradually decrease from T-50 to T-450. Therefore, it also testify that the adsorption capacity of MB onto TiO₂ gradually decrease with the increase of temperature.

According to the characterization of the FT-IR, the organic moieties, such as carboxyl and hydroxyl group, are lost with the calcination temperature increasing. Meanwhile, the zeta potential results also showed that there are some free carboxyl groups not forming the bridging coordination, which makes the TiO₂ samples negative charge at lower calcination temperature. It is reported that the organic moieties on the surface of the TiO₂ samples can interact with MB by the electrostatic attraction and electron donor-acceptor interaction.^[15] In this study, the TiO₂ samples were prepared in the critic acid solution. There are abundant carboxyl and hydroxyl groups on the surface of the as-prepared TiO₂ at lower temperature. Therefore, these TiO₂ samples exhibited excellent adsorption capacity for MB. With the increase of the calcination temperature, the carboxyl and hydroxyl groups disappeared, which lead to the loss of the MB adsorption capacity. This phenomenon indicates that the organic moieties on the surface of the TiO₂ samples are the key roles for the adsorption of MB.

Conclusions

The effects for the interfacial organic groups of the TiO₂ prepared at the different calcination temperatures on the adsorption of the cationic dye MB are investigated in this study. The organic groups in the TiO₂, including carboxyl and hydroxyl groups, are gradually reduced with the increasing calcination temperature. These interfacial functional groups greatly influenced the adsorption capacity of the as-prepared TiO₂ for MB. The adsorption capacity of the TiO₂ samples calcined at 50°C was up to 468.24 mg/g for MB, which was a promising excellent adsorbent. Meanwhile, this value experienced a sharp decline to 33.39 mg/g when the calcination temperature increased up to 250°C. These results suggested that the interfacial organic functional groups were the main adsorption site to the cationic dye MB and the high temperature would destroy these groups and further made the adsorption performance drastically decrease.

Conflict of interest

The authors declare that they have no conflict of interest.

Funding

This study was funded by the National Natural Science Foundation of China (grant number 21307098 and 21507104), the Shaanxi Key Research and Development Program, China (grant number 2017SF-386), and the Fundamental Research Funds for the Central Universities of China.

References

- [1] Wu, H.H.; Gong, Q.H.; Olson, D.H.; Li, J. (2012). Commensurate adsorption of hydrocarbons and alcohols in microporous metal organic frameworks. *Chemical Reviews*, 112 (2): 836–868. doi: [10.1021/cr200216x](https://doi.org/10.1021/cr200216x).
- [2] Hadi, P.; Guo, J.X.; Barford, J.; McKay, G. (2016). Multilayer dye adsorption in activated carbons-facile approach to exploit vacant sites and interlayer charge interaction. *Environmental Science & Technology*, 50 (10): 5041–5049. doi: [10.1021/acs.est.6b00021](https://doi.org/10.1021/acs.est.6b00021).
- [3] Sarker, M.; Bhadra, B.N.; Seo, P.W.; Jhung, S.H. (2017). Adsorption of benzotriazole and benzimidazole from water over a Co-based metal azolate framework MAF-5 (Co). *Journal of Hazardous Materials*, 324: 131–138. doi: [10.1016/j.jhazmat.2016.10.042](https://doi.org/10.1016/j.jhazmat.2016.10.042).
- [4] Apul, O.G.; Karanfil, T. (2015). Adsorption of synthetic organic contaminants by carbon nanotubes: A critical review. *Water Research*, 68: 34–55. doi: [10.1016/j.watres.2014.09.032](https://doi.org/10.1016/j.watres.2014.09.032).
- [5] Crini, G.; Badot, P.-M. (2008). Application of chitosan, a natural aminopolysaccharide, for dye removal from aqueous solutions by adsorption processes using batch studies: A review of recent literature. *Progress in Polymer Science*, 33 (4): 399–447. doi: [10.1016/j.progpolymsci.2007.11.001](https://doi.org/10.1016/j.progpolymsci.2007.11.001).
- [6] Yu, M.; Li, J.; Wang, L.J. (2017). KOH-activated carbon aerogels derived from sodium carboxymethyl cellulose for high-performance supercapacitors and dye adsorption. *Chemical Engineering Journal*, 310: 300–306. doi: [10.1016/j.cej.2016.10.121](https://doi.org/10.1016/j.cej.2016.10.121).
- [7] Liu, J.; Hu, Z.Y.; Peng, Y.; Huang, H.W.; Li, Y.; Wu, M.; Ke, X.X.; Van Tendeloo, G.; Su, B.L. (2016). 2D ZnO mesoporous single-crystal nanosheets with exposed {0001} polar facets for the depollution of cationic dye molecules by highly selective adsorption and photocatalytic decomposition. *Applied Catalysis B-Environmental Journal*, 181: 138–145. doi: [10.1016/j.apcatb.2015.07.054](https://doi.org/10.1016/j.apcatb.2015.07.054).
- [8] Pereira, M.F.R.; Soares, S.F.; Orfao, J.J.M.; Figueiredo, J.L. (2003). Adsorption of dyes on activated carbons: influence of surface chemical groups. *Carbon*, 41 (4): 811–821. doi: [10.1016/S0008-6223\(02\)00406-2](https://doi.org/10.1016/S0008-6223(02)00406-2).
- [9] Guedidi, H.; Reinert, L.; L  v  que, J.-M.; Soneda, Y.; Bellakhal, N.; Duclaux, L. (2013). The effects of the surface oxidation of activated carbon, the solution pH and the temperature on adsorption of ibuprofen. *Carbon*, 54: 432–443. doi: [10.1016/j.carbon.2012.11.059](https://doi.org/10.1016/j.carbon.2012.11.059).
- [10] Bhatnagar, A.; Hogland, W.; Marques, M.; Sillanp  a, M. (2013). An overview of the modification methods of activated carbon for its water treatment applications. *Chemical Engineering Journal*, 219: 499–511. doi: [10.1016/j.cej.2012.12.038](https://doi.org/10.1016/j.cej.2012.12.038).
- [11] Xue, G.; Liu, H.H.; Chen, Q.Y.; Hills, C.; Tyrer, M.; Innocent, F. (2011). Synergy between surface adsorption and photocatalysis during degradation of humic acid on TiO₂/activated carbon composites. *Journal of Hazardous Materials*, 186 (1): 765–772. doi: [10.1016/j.jhazmat.2010.11.063](https://doi.org/10.1016/j.jhazmat.2010.11.063).
- [12] Li, G.Z.; Park, S.; Kang, D.W.; Krajmalnik-Brown, R.; Rittmann, B.E. (2011). 2,4,5-trichlorophenol degradation using a novel TiO₂-coated biofilm carrier: roles of adsorption, photocatalysis, and biodegradation. *Environmental Science & Technology*, 45 (19): 8359–8367. doi: [10.1021/es2016523](https://doi.org/10.1021/es2016523).
- [13] Janus, M.; Kusiak, E.; Choina, J.; Ziebro, J.; Morawski, A. W. (2009). Enhanced adsorption of two azo dyes produced by carbon modification of TiO₂. *Desalination*, 249 (1): 359–363. doi: [10.1016/j.desal.2009.04.013](https://doi.org/10.1016/j.desal.2009.04.013).
- [14] Wang, Q.; Chen, C.; Zhao, D.; Ma, W.; Zhao, J. (2008). Change of adsorption modes of dyes on fluorinated TiO₂ and its effect on photocatalytic degradation of dyes under visible irradiation. *Langmuir*, 24 (14): 7338–7345. doi: [10.1021/la800313s](https://doi.org/10.1021/la800313s).
- [15] Nguyen-Le, M.T.; Lee, B.K. (2015). High temperature synthesis of interfacial functionalized carboxylate mesoporous TiO₂ for effective adsorption of cationic dyes. *Chemical Engineering Journal*, 281: 20–33. doi: [10.1016/j.cej.2015.06.075](https://doi.org/10.1016/j.cej.2015.06.075).
- [16] Feng, J.; Chen, J.; Wang, N.; Li, J.; Shi, J.; Yan, W. (2016). Enhanced adsorption capacity of polypyrrole/TiO₂ composite modified by carboxylic acid with hydroxyl group. *RSC Advances*, 6 (48): 42572–42580. doi: [10.1039/C6RA06738G](https://doi.org/10.1039/C6RA06738G).
- [17] Ojam  e, L.; Aulin, C.; Pedersen, H.; K  ll, P.-O. (2006). IR and quantum-chemical studies of carboxylic acid and glycine adsorption on rutile TiO₂ nanoparticles. *Journal of Colloid and Interface Science*, 296 (1): 71–78. doi: [10.1016/j.jcis.2005.08.037](https://doi.org/10.1016/j.jcis.2005.08.037).
- [18] Kasar, S.; Kumar, S.; Raut, V.V.; Jeyakumar, S.; Tomar, B.S. (2015). Speciation of citric acid on anatase (TiO₂)-water interface and its effect on Eu(III) sorption. *Radiochimica Acta*, 103 (4): 305–312. doi: [10.1515/ract-2014-2320](https://doi.org/10.1515/ract-2014-2320).
- [19] Wu, H.; Ma, J.; Zhang, C.; He, H. (2014). Effect of TiO₂ calcination temperature on the photocatalytic oxidation of gaseous NH₃. *Journal of Environmental Sciences*, 26 (3): 673–682. doi: [10.1016/S1001-0742\(13\)60441-6](https://doi.org/10.1016/S1001-0742(13)60441-6).
- [20] Kim, L.J.; Jang, J.W.; Park, J.W. (2014). Nano TiO₂--functionalized magnetic-cored dendrimer as a photocatalyst. *Applied Catalysis B-Environmental Journal*, 147: 973–979. doi: [10.1016/j.apcatb.2013.10.024](https://doi.org/10.1016/j.apcatb.2013.10.024).
- [21] Yu, H.G.; Xiao, P.; Tian, J.; Wang, F.Z.; Yu, J.G. (2016). Phenylamine-functionalized rGO/TiO₂ photocatalysts: spatially separated adsorption sites and tunable photocatalytic selectivity. *ACS Applied Materials & Interfaces*, 8 (43): 29470–29477. doi: [10.1021/acsami.6b09903](https://doi.org/10.1021/acsami.6b09903).
- [22] Kheirandish, S.; Ghaedi, M.; Dashtian, K.; Jannesar, R.; Montazerzohori, M.; Pourebrahim, F.; Zare, M.A. (2017). Simultaneous removal of Cd(II), Ni(II), Pb(II) and Cu(II) ions via their complexation with HBANSA based on a combined ultrasound-assisted and cloud point adsorption method using CSG-BiPO₄/FePO₄ as

- novel adsorbent: FAAS detection and optimization process. *Journal of Colloid and Interface Science*, 500: 241–252. doi: [10.1016/j.jcis.2017.03.070](https://doi.org/10.1016/j.jcis.2017.03.070).
- [23] Pourebrahim, F.; Ghaedi, M.; Dashtian, K.; Heidari, F.; Kheirandish, S. (2017). Simultaneous removing of Pb^{2+} ions and alizarin red S dye after their complexation by ultrasonic waves coupled adsorption process: spectrophotometry detection and optimization study. *Ultrasonics Sonochemistry*, 35: 51–60. doi: [10.1016/j.ultsonch.2016.09.002](https://doi.org/10.1016/j.ultsonch.2016.09.002).
- [24] Dashtian, K.; Zare-Dorabei, R. (2017). Synthesis and characterization of functionalized mesoporous SBA-15 decorated with Fe_3O_4 nanoparticles for removal of Ce(III) ions from aqueous solution: ICP-OES detection and central composite design optimization. *Journal of Colloid and Interface Science*, 494: 114–123. doi: [10.1016/j.jcis.2017.01.072](https://doi.org/10.1016/j.jcis.2017.01.072).
- [25] Azad, F.N.; Ghaedi, M.; Dashtian, K.; Jamshidi, A.; Hassani, G.; Montazerzohori, M.; Hajati, S.; Rajabi, M.; Bazrafshan, A.A. (2016). Preparation and characterization of an AC- Fe_3O_4 -Au hybrid for the simultaneous removal of Cd^{2+} , Pb^{2+} , Cr^{3+} and Ni^{2+} ions from aqueous solution via complexation with 2-((2,4-dichloro-benzylidene)-amino)-benzenethiol: taguchi optimization. *RSC Advances*, 6 (24): 19780–19791. doi: [10.1039/C6RA01910B](https://doi.org/10.1039/C6RA01910B).
- [26] Jamshidi, M.; Ghaedi, M.; Dashtian, K.; Ghaedi, A.M.; Hajati, S.; Goudarzi, A.; Alipanahpour, E. (2016). Highly efficient simultaneous ultrasonic assisted adsorption of brilliant green and eosin B onto ZnS nanoparticles loaded activated carbon: artificial neural network modeling and central composite design optimization. *Spectrochimica Acta Part A: Molecular and Biomolecular Spectroscopy*, 153: 257–267. doi: [10.1016/j.saa.2015.08.024](https://doi.org/10.1016/j.saa.2015.08.024).
- [27] Nasiri Azad, F.; Ghaedi, M.; Dashtian, K.; Montazerzohori, M.; Hajati, S.; Alipanahpour, E. (2015). Preparation and characterization of MWCNTs functionalized by N-(3-nitrobenzylidene)-N'-trimethoxysilylpropyl-ethane-1,2-diamine for the removal of aluminum(iii) ions via complexation with eriochrome cyanine R: spectrophotometric detection and optimization. *RSC Advances*, 5 (75): 61060–61069. doi: [10.1039/C5RA08746E](https://doi.org/10.1039/C5RA08746E).
- [28] Jamshidi, M.; Ghaedi, M.; Dashtian, K.; Hajati, S. (2015). New ion-imprinted polymer-functionalized mesoporous SBA-15 for selective separation and preconcentration of Cr(iii) ions: modeling and optimization. *RSC Advances*, 5 (128): 105789–105799. doi: [10.1039/C5RA17873H](https://doi.org/10.1039/C5RA17873H).
- [29] Nasiri Azad, F.; Ghaedi, M.; Dashtian, K.; Jamshidi, A.; Hassani, G.; Montazerzohori, M.; Hajati, S.; Rajabi, M.; Bazrafshan, A.A. (2016). Preparation and characterization of an AC- Fe_3O_4 -Au hybrid for the simultaneous removal of Cd^{2+} , Pb^{2+} , Cr^{3+} and Ni^{2+} ions from aqueous solution via complexation with 2-((2,4-dichloro-benzylidene)-amino)-benzenethiol: taguchi optimization. *RSC Advances*, 6 (24): 19780–19791. doi: [10.1039/C6RA01910B](https://doi.org/10.1039/C6RA01910B).
- [30] Asfaram, A.; Ghaedi, M.; Dashtian, K.; Ghezelbash, G. R. (2018). Preparation and characterization of $\text{Mn}_{0.4}\text{Zn}_{0.6}\text{Fe}_2\text{O}_4$ nanoparticles supported on dead cells of *Yarrowia lipolytica* as a novel and efficient adsorbent/biosorbent composite for the removal of azo food dyes: central composite design optimization study. *ACS Sustainable Chemistry & Engineering*, 6 (4): 4549–4563. doi: [10.1021/acssuschemeng.7b03205](https://doi.org/10.1021/acssuschemeng.7b03205).
- [31] Ghaedi, M.; Azad, F.N.; Dashtian, K.; Hajati, S.; Goudarzi, A.; Soylak, M. (2016). Central composite design and genetic algorithm applied for the optimization of ultrasonic-assisted removal of malachite green by ZnO nanorod-loaded activated carbon. *Spectrochimica Acta Part A: Molecular and Biomolecular Spectroscopy*, 167: 157–164. doi: [10.1016/j.saa.2016.05.025](https://doi.org/10.1016/j.saa.2016.05.025).
- [32] Jankovic, I.A.; Saponjic, Z.V.; Comor, M.I.; Nedeljkovic, J.M. (2009). Surface modification of colloidal TiO_2 nanoparticles with bidentate benzene derivatives. *Journal of Physical Chemistry C*, 113 (29): 12645–12652. doi: [10.1021/jp9013338](https://doi.org/10.1021/jp9013338).
- [33] Yost, E.C.; Tejedortejedor, M.I.; Anderson, M.A. (1990). INSITU CIR-FTIR CHARACTERIZATION OF SALICYLATE COMPLEXES AT THE GOETHITE AQUEOUS-SOLUTION INTERFACE. *Environmental Science & Technology*, 24 (6): 822–828. doi: [10.1021/es00076a005](https://doi.org/10.1021/es00076a005).
- [34] Blinova, N.V.; Stejskal, J.; Trchova, M.; Prokes, J.; Omastova, M. (2007). Polyaniline and polypyrrole: a comparative study of the preparation. *European Polymer Journal*, 43 (6): 2331–2341. doi: [10.1016/j.eurpolymj.2007.03.045](https://doi.org/10.1016/j.eurpolymj.2007.03.045).
- [35] Jafari, B.; Rahimi, M.R.; Ghaedi, M.; Dashtian, K.; Mosleh, S. (2018). CO_2 capture by amine-based aqueous solution containing atorvastatin functionalized mesocellular silica foam in a counter-current rotating packed bed: central composite design modeling. *Chemical Engineering Research and Design*, 129: 64–74. doi: [10.1016/j.cherd.2017.11.005](https://doi.org/10.1016/j.cherd.2017.11.005).
- [36] Mosleh, S.; Rahimi, M.R.; Ghaedi, M.; Dashtian, K.; Hajati, S. (2018). Sonochemical-assisted synthesis of $\text{CuO/Cu}_2\text{O/Cu}$ nanoparticles as efficient photocatalyst for simultaneous degradation of pollutant dyes in rotating packed bed reactor: LED illumination and central composite design optimization. *Ultrasonics Sonochemistry*, 40: 601–610. doi: [10.1016/j.ultsonch.2017.08.007](https://doi.org/10.1016/j.ultsonch.2017.08.007).
- [37] Mosleh, S.; Rahimi, M.R.; Ghaedi, M.; Dashtian, K.; Hajati, S. (2016). Photocatalytic degradation of binary mixture of toxic dyes by HKUST-1 MOF and HKUST-1-SBA-15 in a rotating packed bed reactor under blue LED illumination: central composite design optimization. *RSC Advances*, 6 (21): 17204–17214. doi: [10.1039/C5RA24564H](https://doi.org/10.1039/C5RA24564H).
- [38] Mousavinia, S.E.; Hajati, S.; Ghaedi, M.; Dashtian, K. (2016). Novel nanorose-like Ce(III)-doped and undoped $\text{Cu(II)-biphenyl-4,4-dicarboxylic acid (Cu(II)-BPDCa)}$ MOFs as visible light photocatalysts: synthesis, characterization, photodegradation of toxic dyes and optimization. *Physical Chemistry Chemical Physics: PCCP*, 18 (16): 11278–11287. doi: [10.1039/c6cp00910g](https://doi.org/10.1039/c6cp00910g).
- [39] Ahmad, R.; Mirza, A. (2017). Synthesis of guar gum/bentonite a novel bionanocomposite: isotherms, kinetics and thermodynamic studies for the removal of Pb (II) and crystal violet dye. *Journal of Molecular Liquids*, 249: 805–814. doi: [10.1016/j.molliq.2017.11.082](https://doi.org/10.1016/j.molliq.2017.11.082).

- [40] Ahmad, R.; Mirza, A. (2017). Green synthesis of xanthan gum/methionine-bentonite nanocomposite for sequestering toxic anionic dye. *Surfaces & Interfaces*, 8: 65–72. doi: [10.1016/j.surfin.2017.05.001](https://doi.org/10.1016/j.surfin.2017.05.001).
- [41] Li, X.Y.; Wang, D.S.; Cheng, G.X.; Luo, Q.Z.; An, J.; Wang, Y.H. (2008). Preparation of polyaniline-modified TiO₂ nanoparticles and their photocatalytic activity under visible light illumination. *Applied Catalysis B-Environmental Journal*, 81 (3–4): 267–273. doi: [10.1016/j.apcatb.2007.12.022](https://doi.org/10.1016/j.apcatb.2007.12.022).
- [42] Mosleh, S.; Rahimi, M.R.; Ghaedi, M.; Dashtian, K.; Hajati, S.; Wang, S. (2017). Ag₃PO₄/AgBr/Ag-HKUST-1-MOF composites as novel blue LED light active photocatalyst for enhanced degradation of ternary mixture of dyes in a rotating packed bed reactor. *Chemical Engineering and Processing: Process Intensification*, 114: 24–38. doi: [10.1016/j.cep.2017.01.009](https://doi.org/10.1016/j.cep.2017.01.009).
- [43] Mosleh, S.; Rahimi, M.R.; Ghaedi, M.; Dashtian, K.; Hajati, S. (2016). BiPO₄/Bi₂S₃-HKUST-1-MOF as a novel blue light-driven photocatalyst for simultaneous degradation of toluidine blue and auramine-O dyes in a new rotating packed bed reactor: optimization and comparison to a conventional reactor. *RSC Advances*, 6 (68): 63667–63680. doi: [10.1039/C6RA10385E](https://doi.org/10.1039/C6RA10385E).
- [44] Chun, Y.; Sheng, G.Y.; Chiou, C.T.; Xing, B.S. (2004). Compositions and sorptive properties of crop residue-derived chars. *Environmental Science & Technology*, 38 (17): 4649–4655.
- [45] Vathyam, R.; Wondimu, E.; Das, S.; Zhang, C.; Hayes, S.; Tao, Z.M.; Asefa, T. (2011). Improving the adsorption and release capacity of organic-functionalized mesoporous materials to drug molecules with temperature and synthetic methods. *Journal of Physical Chemistry C*, 115 (27): 13135–13150. doi: [10.1021/jp1108587](https://doi.org/10.1021/jp1108587).
- [46] Yu, J.C.; Yu, J.G.; Ho, W.K.; Jiang, Z.T.; Zhang, L.Z. (2002). Effects of F[−] doping on the photocatalytic activity and microstructures of nanocrystalline TiO₂ powders. *Chemistry of Materials*, 14 (9): 3808–3816. doi: [10.1021/cm020027c](https://doi.org/10.1021/cm020027c).
- [47] Yu, J.C.; Yu, J.G.; Ho, W.K.; Zhang, L.Z. (2001). Preparation of highly photocatalytic active nano-sized TiO₂ particles via ultrasonic irradiation. *Chem Communications*, (19): 1942–1943. doi: [10.1039/b105471f](https://doi.org/10.1039/b105471f).
- [48] Grosso, D.; Soler-Illia, G.; Crepaldi, E.L.; Cagnol, F.; Sinturel, C.; Bourgeois, A.; Brunet-Bruneau, A.; Amenitsch, H.; Albouy, P.A.; Sanchez, C. (2003). Highly porous TiO₂ anatase optical thin films with cubic mesostructure stabilized at 700 degrees C. *Chemistry of Materials*, 15 (24): 4562–4570. doi: [10.1021/cm031060h](https://doi.org/10.1021/cm031060h).
- [49] Yang, H.G.; Zeng, H.C. (2004). Preparation of hollow anatase TiO₂ nanospheres via Ostwald ripening. *Journal of Physical Chemistry B*, 108 (11): 3492–3495. doi: [10.1021/jp0377782](https://doi.org/10.1021/jp0377782).
- [50] Dai, Y.Q.; Cobley, C.M.; Zeng, J.; Sun, Y.M.; Xia, Y.N. (2009). Synthesis of anatase TiO₂ nanocrystals with exposed {001} facets. *Nano Letters*, 9 (6): 2455–2459. doi: [10.1021/nl901181n](https://doi.org/10.1021/nl901181n).
- [51] Feng, J.T.; Zhu, J.W.; Lv, W.; Li, J.J.; Yan, W. (2015). Effect of hydroxyl group of carboxylic acids on the adsorption of acid red G and methylene blue on TiO₂. *Chemical Engineering Journal*, 269: 316–322. doi: [10.1016/j.cej.2015.01.109](https://doi.org/10.1016/j.cej.2015.01.109).
- [52] Peng, S.; Wang, S.; Chen, T.; Jiang, S.; Huang, C. (2010). Adsorption kinetics of methylene blue from aqueous solutions onto palygorskite. *Acta Geologica Sinica*, 80 (2): 236–242. doi: [10.1111/j.1755-6724.2006.tb00236.x](https://doi.org/10.1111/j.1755-6724.2006.tb00236.x).
- [53] Yao, S.; Lai, H.; Shi, Z. (2012). Biosorption of methyl blue onto tartaric acid modified wheat bran from aqueous solution. *Iranian Journal of Environmental Health Science & Engineering*, 9 (1): 16. doi: [10.1186/1735-2746-9-16](https://doi.org/10.1186/1735-2746-9-16).
- [54] Zhang, L.Y.; Zhang, W.; Zhou, Z.; Li, C.M. (2016). gamma-Fe₂O₃ nanocrystals-anchored macro/meso-porous graphene as a highly efficient adsorbent toward removal of methylene blue. *Journal of Colloid and Interface Science*, 476: 200–205. doi: [10.1016/j.jcis.2016.05.025](https://doi.org/10.1016/j.jcis.2016.05.025).
- [55] Zhan, H.; Jiang, Y.; Ma, Q. (2014). Determination of adsorption characteristics of metal oxide nanomaterials: application as adsorbents. *Analytical Letters*, 47 (5): 871–884. doi: [10.1080/00032719.2013.850090](https://doi.org/10.1080/00032719.2013.850090).
- [56] Wang, S.; Li, L.; Wu, H.; Zhu, Z.H. (2005). Unburned carbon as a low-cost adsorbent for treatment of methylene blue-containing wastewater. *Journal of Colloid and Interface Science*, 292 (2): 336–343. doi: [10.1016/j.jcis.2005.06.014](https://doi.org/10.1016/j.jcis.2005.06.014).
- [57] Rao, V.V.B.; Rao, S.R.M. (2006). Adsorption studies on treatment of textile dyeing industrial effluent by flyash. *Chemical Engineering Journal*, 116 (1): 77–84. doi: [10.1016/j.cej.2005.09.029](https://doi.org/10.1016/j.cej.2005.09.029).
- [58] Mazaheri, H.; Ghaedi, M.; Hajati, S.; Dashtian, K.; Purkait, M.K. (2015). Simultaneous removal of methylene blue and Pb²⁺ ions using ruthenium nanoparticle-loaded activated carbon: response surface methodology. *RSC Advances*, 5 (101): 83427–83435. doi: [10.1039/C5RA06731F](https://doi.org/10.1039/C5RA06731F).
- [59] Li, P.H.Y.; Bruce, R.L.; Hobday, M.D. (2015). A pseudo first order rate model for the adsorption of an organic adsorbate in aqueous solution. *Journal of Chemical Technology & Biotechnology*, 74 (1): 55–59. doi: [10.1002/\(SICI\)1097-4660\(199901\)74:1<55::AID-JCTB984>3.0.CO;2-D](https://doi.org/10.1002/(SICI)1097-4660(199901)74:1<55::AID-JCTB984>3.0.CO;2-D).
- [60] Tijani, J.O.; Bankole, M.T.; Muriana, M.; Falana, I.O. (2014). Development of low cost adsorbent from cow horn for the biosorption of Mn (II), Ni (II) and Cd (II) ion from aqueous solution. *Research Journal of Applied Sciences Engineering & Technology*, 7 (1): 9–17. doi: [10.19026/rjaset.7.213](https://doi.org/10.19026/rjaset.7.213).
- [61] Wang, N.; Feng, J.; Chen, J.; Wang, J.; Yan, W. (2017). Adsorption mechanism of phosphate by polyaniline/TiO₂ composite from wastewater. *Chemical Engineering Journal*, 316: 33–40.
- [62] Abdi, S.; Nasiri, M.; Mesbahi, A.; Khani, M.H. (2017). Investigation of uranium (VI) adsorption by polypyrrole. *Journal of Hazardous Materials*, 332: 132–139. doi: [10.1016/j.jhazmat.2017.01.013](https://doi.org/10.1016/j.jhazmat.2017.01.013).
- [63] Hossain, M.K.; Pervez, M.F.; Uddin, M.J.; Tayyaba, S.; Mia, M.N.H.; Bashar, M.S.; Jewel, M.K. H.; Haque, M.A.S.; Hakim, M.A.; Khan, M.A. (2018). Influence of natural dye adsorption on the structural, morphological and optical properties of TiO₂ based photoanode of dye-sensitized solar cell. *Materials Science-Poland*, 36 (1): 93–101. doi: [10.1515/msp-2017-0090](https://doi.org/10.1515/msp-2017-0090).